INTERNATIONAL JOURNAL OF ROBUST AND NONLINEAR CONTROL
Int. J. Robust Nonlinear Control 2014; **24**:644–668
Published online 16 October 2012 in Wiley Online Library (wileyonlinelibrary.com). DOI: 10.1002/rnc.2910

An asymptotically stable sensorless speed controller for non-salient permanent magnet synchronous motors

D. Shah[1], G. Espinosa–Pérez[2,*,†], R. Ortega[1] and M. Hilairet[3]

[1]*Laboratoire des Signaux et Systèmes, CNRS–SUPELEC, 91192 Gif–sur–Yvette, France*
[2]*Facultad de Ingeniería–UNAM, Edificio Posgrado 2do. piso, Ciudad Universitaria, 04510 México D.F., Mexico*
[3]*Laboratoire de Genie Electrique de Paris, CNRS–SUPELEC, 91192 Gif–sur–Yvette, France*

SUMMARY

A solution to the longstanding problem of sensorless control of an electrical machine is provided in this paper. That is, the construction of an asymptotically stable controller that regulates the mechanical speed of the motor, measuring only the electrical coordinates. The result is presented for a non-salient permanent magnet synchronous motor perturbed by an unknown constant load torque. The proposed scheme is a fourth order nonlinear observer-based controller that does not rely on—intrinsically nonrobust—operations like open-loop integration of the systems dynamical model nor signal differentiation and can be easily implemented in real time. The controller is easy to commission, with the tuning gains directly determining the convergence rates of the position, speed, and load torque observers. Simulation and experimental results are presented. In particular, a comparison with a sensorless field-oriented controller, recently proposed in the drives literature, is carried out. Copyright © 2012 John Wiley & Sons, Ltd.

Received 23 September 2011; Revised 24 August 2012; Accepted 30 August 2012

KEY WORDS: sensorless control; electrical machines; permanent magnet synchronous motors

1. INTRODUCTION

Control of electrical machines is a topic that has attracted the attention of the control community for many years now, see [1] for an early influential reference. Rigorous mathematical analysis of the usual strategies applied in industrial applications and the proposition of novel control schemes have been reported in the literature [2–5]. In this paper, we are interested in the challenging problem of eliminating the use of sensors for the mechanical variables (position and speed), the so-called *sensorless control* [6], for non-salient permanent magnet synchronous motors (PMSM).

For successful sensorless speed control of PMSMs, three variables must be estimated out of the measurement of the electrical coordinates: rotor position and speed, and load torque—the latter assumed constant. Broadly speaking, there are three approaches to rotor position estimation of PMSMs reported in the literature. In the first approach, position information is obtained by using high-frequency electrical variables, for example, injecting high-frequency signals of voltages or currents, whereas in the second one, this is carried out using information obtained from the fundamental components of voltage and current signals,for example, analyzing the electromotive force. The third, more classical, approach implements extended Kalman filters that aim at estimating the full state of the machine. See [7] for further details on the classification of the two first approaches as well as a list of relevant related references and [8] for a recent illustrative reference of the third approach. For non-salient pole PMSMs (also known as ‘surface mounted’ PMSMs), the second

*Correspondence to: G. Espinosa–Pérez, Facultad de Ingeniería–UNAM, Edificio Posgrado 2do. piso, Ciudad Universitaria, 04510 México D.F., Mexico.
†E-mail: gerardoe@unam.mx

approach, which is based on the estimation of the back-emf force induced by the permanent magnets, is the simplest and most common and is the one adopted in this paper.

As explained in [4, 7, 9], standard back-emf estimation methods are difficult to tune for standstill and low-speed regimes because the designs are based on linear approximations of the highly nonlinear first principles model. A notable exception to this linearization-based approach is the pioneering work reported in [10]. In [9], a globally (under some conditions, even exponentially) stable position observer for PMSMs is reported. The analysis, performed for the full nonlinear model, yields very simple robust tuning rules. In [11], the position observer was combined with an *ad hoc* linear speed estimator and a standard field-oriented controller, which are often used in applications, yielding very encouraging experimental results—see also the recent book [4]. However, no theoretical justification was provided for the overall observer-controller scheme. The main objective of this paper is to prove that direct application of two well-established design methodologies—immersion and invariance (I&I) [12] for the observer, and interconnection and damping assignment passivity-based control (IDA-PBC) [13] for the control—can be combined with the observer of [9] to design an asymptotically stable sensorless controller. The result builds upon some preliminary work reported in [9, 14] where, assuming *position is known*, I&I techniques are used to design a speed and load torque observer, and in [15, 16] where *full state-feedback*, globally convergent, IDA-PBCs for the PMSM are proposed.

To the best of our knowledge, this is the first time a complete theoretical analysis of a sensorless controller is performed—under reasonable practical and theoretical assumptions. Heuristically conceived schemes abound in the literature (see, e.g., [7, 17] for recent surveys). Many results are also available for the (practically unrealistic) cases of known initial position [18, 19] or zero load torque [20], or the (theoretically unjustifiable) assumption of bounded trajectories [18]. An approximate stability analysis of the scheme proposed in [10] is carried out in [21]. In [22], a probably stable sensorless scheme for wound rotor synchronous motors is proposed. A key difference of the latter machine with the PMSM is the availability of flux measurements that considerably simplifies the observation problem. The observability properties of PMSMs have been recently studied in [9, 20] and for induction machines in [23] and [24]. In [25], it is shown that the standard PBC controller for induction machines of [26], see also [5], verifies an input-to-state stability property with respect to the estimation errors.

The remaining of the paper is organized as follows. The models of the PMSM and the problem formulation are given in Section 2. The controller structure and the main result are presented in Section 3. In Section 4, the particular stability properties of the full information IDA-PBC, the position observer of [9], and the I&I speed and load torque observer are briefly revised. Some simulation and experimental results are given in Section 5, including a comparison with the heuristic controller of [11]. Finally, we wrap-up the paper with concluding remarks in Section 6.

2. PMSM MODELS AND PROBLEM FORMULATION

2.1. $\alpha\beta$ model of the PMSM

The classical fixed-frame ($\alpha\beta$) model of the unsaturated non-salient PMSM is given in [27, 28]

$$\begin{aligned} L\frac{\mathrm{d}i_{\alpha\beta}}{\mathrm{d}t} &= -Ri_{\alpha\beta} - n_p\omega\Phi\mathcal{J}\begin{bmatrix}\cos(\theta)\\ \sin(\theta)\end{bmatrix} + v_{\alpha\beta}\\ J\dot{\omega} &= n_p\Phi i_{\alpha\beta}^{\top}\mathcal{J}\begin{bmatrix}\cos(\theta)\\ \sin(\theta)\end{bmatrix} - \tau_L\\ \dot{\theta} &= n_p\omega, \end{aligned} \tag{1}$$

where $\mathcal{J} := \begin{bmatrix}0 & -1\\ 1 & 0\end{bmatrix}$, $i_{\alpha\beta} = \begin{bmatrix}i_\alpha\\ i_\beta\end{bmatrix}$ and $v_{\alpha\beta} = \begin{bmatrix}v_\alpha\\ v_\beta\end{bmatrix}$ are the stator currents and motor terminal voltages, respectively, ω is the rotor angular velocity, with $\frac{1}{n_p}\theta$ the corresponding position, L is the stator inductance, R is the stator resistance, n_p is the number of pole pairs, J is the moment

DOI: 10.1002/rnc

of inertia (normalized with n_p), Φ is the magnetic flux and τ_L is the load torque, which is assumed *constant*, but unknown.

To design the observer, it is convenient to embed the dynamics (1) into the higher-dimensional system

$$L\frac{\mathrm{d}i_{\alpha\beta}}{\mathrm{d}t} = -Ri_{\alpha\beta} - n_p\omega\Phi\mathcal{J}\rho_{\alpha\beta} + v_{\alpha\beta} \tag{2}$$

$$J\dot{\omega} = n_p\Phi i_{\alpha\beta}^{\top}\mathcal{J}\rho_{\alpha\beta} - \tau_L \tag{3}$$

$$\dot{\rho}_{\alpha\beta} = n_p\omega\mathcal{J}\rho_{\alpha\beta}, \tag{4}$$

where the vector

$$\rho_{\alpha\beta} := \begin{bmatrix} \rho_\alpha \\ \rho_\beta \end{bmatrix} = \begin{bmatrix} \cos(\theta) \\ \sin(\theta) \end{bmatrix} \tag{5}$$

is defined. Notice that, if $\rho_{\alpha\beta}$ is known, θ can be easily reconstructed inverting the trigonometric functions.

2.2. *dq model of the PMSM*

The model (1) can be written in rotating (dq) coordinates by means of the transformation

$$e^{\mathcal{J}\theta} = \begin{bmatrix} \cos(\theta) & -\sin(\theta) \\ \sin(\theta) & \cos(\theta) \end{bmatrix} = \rho_\alpha I_2 + \rho_\beta\mathcal{J}, \tag{6}$$

with I_2 the 2×2 identity matrix, to obtain

$$\begin{aligned} L\frac{\mathrm{d}i}{\mathrm{d}t} &= -(RI_2 + n_p\omega L\mathcal{J})i - n_p\omega\Phi\mathcal{J}e_1 + v \\ J\dot{\omega} &= n_p\Phi i_2 - \tau_L \\ \dot{\theta} &= n_p\omega, \end{aligned} \tag{7}$$

where the rotated signals

$$i = \begin{bmatrix} i_1 \\ i_2 \end{bmatrix} := e^{-\mathcal{J}\theta}i_{\alpha\beta},\ v = \begin{bmatrix} v_1 \\ v_2 \end{bmatrix} := e^{-\mathcal{J}\theta}v_{\alpha\beta},\ e_1 = \begin{bmatrix} 1 \\ 0 \end{bmatrix} := e^{-\mathcal{J}\theta}\rho_{\alpha\beta} \tag{8}$$

are defined.

Remark 1
The main advantage of the dq-model is that it transforms the periodic orbits associated to the constant speed operation of the $\alpha\beta$ model of the PMSM into equilibrium points.

Remark 2
The assignable equilibrium set for (7) is given by

$$\left\{(i^\star, \omega^\star) \mid i_2^\star = \frac{1}{n_p\Phi}\tau_L\right\}, \tag{9}$$

with $i_1^\star$ and $\omega^\star$ arbitrary. Consistent with engineering practice and centering the interest on low speed operation, we will fix $i_1^\star = 0$ in the sequel.

Remark 3
The industry standard field-oriented control [28] is designed for the dq model; hence, the need to reconstruct θ. Indeed, it must be recalled that the input is $v_{\alpha\beta}$ whereas the measurable output is $i_{\alpha\beta}$, but θ is an *unmeasurable* variable under sensorless operation.

DOI: 10.1002/rnc

2.3. Problem formulation

The main contribution of the paper is the solution of the following.

Sensorless control problem. Consider the PMSM model (2)–(4) and a desired constant speed $\omega^\star \neq 0$, under the following conditions.

A.1 The only variables available for measurement are $i_{\alpha\beta}$.
A.2 The load torque τ_L is constant but *unknown*.
A.3 The parameters R, L, Φ, and J are known.

Design an output-feedback controller that ensures the existence of a set of initial conditions, which guarantees that all signals are bounded and that $\omega(t)$ converges, *exponentially fast*, to $\omega^\star$.

Remark 4
Even though we have restricted to the case of constant desired speed and constant load torque, it is clear that the controller, being exponentially stable hence robust, will be able to track time-varying references and reject changes in the load torque. Proving this fact, for slowly time-varying signals is straightforward doing a singular perturbation analysis. Interestingly, the simulations and experimental results of Section 5 show that the proposed controller yields a good performance even in the face of fast changes in the speed reference and the load torque.

Remark 5
The constraint that $\omega^\star \neq 0$ is necessary in the present (sensorless) context, because it is easy to show (e.g., [9, 20]) that the rank condition for observability is violated when the motor is at standstill.[‡] Although this assumption is not restrictive when sign changes in the desired speed are required, due to the intrinsic robustness of the controller, it is clear that it imposes a limitation when operation at or close to standstill is required for long amounts of time (e.g., hoisting).

3. AN EXPONENTIALLY STABLE SENSORLESS CONTROLLER

To simplify the presentation of the main result, it is convenient to explain the controller structure and define the notation. The proposed controller is a fourth-order certainty-equivalent version of a full-information (based on the complete state $\rho_{\alpha\beta}, \omega, \tau_L, i_{\alpha\beta}$) globally asymptotically stabilizing controller, which is a static state-feedback IDA-PBC. The certainty equivalent version is obtained replacing the unmeasurable state $\rho_{\alpha\beta}, \omega, \tau_L$ by their estimates. The dynamics of the controller is, then, due to the I&I observer previously mentioned in Section 1, which generates the estimates that we denote $\hat{\rho}_{\alpha\beta}, \hat{\omega}, \hat{\tau}_L$, respectively. The controller, combined with the third-order PMSM dynamics (7) yields a seventh-order closed-loop system.

As usual, the analysis is carried out in error coordinates, which is a mixture of regulation errors, $(\cdot) - (\cdot)^\star$, and estimation errors, $\widehat{(\cdot)} - (\cdot)$. To simplify the notation, all these errors are lumped into a seventh–dimensional vector denoted χ, and defined as[§]

$$\chi = \begin{bmatrix} \chi_1 \\ \chi_2 \\ \chi_3 \\ \chi_4 \\ \chi_5 \\ \chi_6 \\ \chi_7 \end{bmatrix} := \begin{bmatrix} L(i - i^\star) \\ J(\omega - \omega^\star) \\ e^{-\mathcal{J}\theta}\left(\hat{\rho}_{\alpha\beta} - \rho_{\alpha\beta}\right) \\ \hat{\omega} - \omega \\ \hat{\tau}_L - \tau_L \end{bmatrix}. \tag{10}$$

Notice that the errors in both, the currents and the vector $\rho_{\alpha\beta}$, are defined in the dq coordinates.

[‡]See [29] for a detailed observability analysis.
[§]The constants L and J are introduced because—consistent with the Hamiltonian formulation—the IDA-PBC is derived with the motor dynamics represented using the energy variables, flux, and momenta.

DOI: 10.1002/rnc

3.1. Main stability result

Our main result is the following proposition, whose proof is given in Subsection 3.2.

Proposition 1
Consider the PMSM model (2)–(4) in closed-loop with the fourth-order observer-based speed regulator

$$v_{\alpha\beta} = \left(\hat{\rho}_\alpha I_2 + \hat{\rho}_\beta \mathcal{J}\right) \hat{v}$$
$$\hat{v} = (R - r)i + \begin{bmatrix} -\frac{L}{\Phi}\hat{\tau}_L \hat{\omega} \\ n_p \Phi \omega^\star + \frac{r}{n_p \Phi}\hat{\tau}_L \end{bmatrix}, \tag{11}$$

where $r > 0$ is a damping injection term, and the estimates are obtained from the position observer

$$\dot{\hat{\lambda}} = -R i_{\alpha\beta} + v_{\alpha\beta} + \gamma \eta(\hat{\lambda}) \left[\Phi^2 - |\eta(\hat{\lambda})|^2\right] \tag{12}$$

$$\hat{\rho}_{\alpha\beta} = \frac{1}{\Phi}\eta(\hat{\lambda}) \tag{13}$$

$$\eta(\hat{\lambda}) = \hat{\lambda} - L i_{\alpha\beta} \tag{14}$$

with $|\cdot|$ the Euclidean norm, and the speed-load torque observer

$$\dot{\xi} = A_{33}\xi + \begin{bmatrix} \frac{a_2}{J} - n_p a_1^2 \\ n_p a_1 a_2 \end{bmatrix} \mathcal{A}\left(\frac{\hat{\rho}_\beta}{\hat{\rho}_\alpha}\right) + \begin{bmatrix} \frac{n_p \Phi}{J} i_{\alpha\beta}^\top \mathcal{J} \hat{\rho}_{\alpha\beta} \\ 0 \end{bmatrix}$$
$$\begin{bmatrix} \hat{\omega} \\ \hat{\tau}_L \end{bmatrix} = \xi + \begin{bmatrix} a_1 \\ -a_2 \end{bmatrix} \mathcal{A}\left(\frac{\hat{\rho}_\beta}{\hat{\rho}_\alpha}\right), \tag{15}$$

where a_1, a_2 are strictly positive constants,

$$A_{33} := \begin{bmatrix} -n_p a_1 & -\frac{1}{J} \\ n_p a_2 & 0 \end{bmatrix}, \tag{16}$$

and $\mathcal{A}(\cdot)$ is an operator defined in Appendix A.[¶] The error signals defined in (10) are described by a differential equation of the form

$$\dot{\chi} = f(\chi), \tag{17}$$

with zero a (locally) *exponentially stable* equilibrium. Consequently, there exist constants m, ϵ, $\alpha > 0$ such that the following implication holds

$$\left(|\chi(0)| \leqslant \epsilon \;\Rightarrow\; |\chi(t)| \leqslant m e^{-\alpha t} |\chi(0)|\right),$$

for all $t \geqslant 0$.

Remark 6
The estimator of $\rho_{\alpha\beta}$ requires the reconstruction of $\hat{\theta}$ via the computation of arctan $\left(\frac{\hat{\rho}_\beta}{\hat{\rho}_\alpha}\right)$—recall the definition (5). As is well known, the arctan function suffers from the drawbacks that it is not defined for $\hat{\rho}_\alpha = 0$ and does not distinguish between diametrically opposite directions (of the vector with coordinates $(\hat{\rho}_\alpha, \hat{\rho}_\beta)$). To overcome these obstacles, the function atan2$(\hat{\rho}_\beta, \hat{\rho}_\alpha)$ is used [30]. Furthermore, in the observer implementation, the derivative of this signal, which is piecewise continuous but not continuous, is required. To avoid the appearance of Dirac delta functions, an operator that 'unwraps' the circle—where $\hat{\theta}$ lives—is introduced. The operator is defined by some lines of code, which are given in Appendix A. Both modifications are well-known, and widely used, in the drives community.

[¶]As explained in Section 4.3, the operator $\mathcal{A}(z)$, which is widely used in the drives community, is 'essentially' equal to arctan(z) and is introduced to avoid singularities and jumps.

DOI: 10.1002/rnc

3.2. *Proof of Proposition 1*

To prove Proposition 1, we first compute the error equations (17). For ease of reference, these equations are sequentially derived for χ_{13}, χ_{45}, and χ_{67}. The stability properties of the system are established invoking Lyapunov's indirect method. Towards this end, the equations are written in the form

$$\dot{\chi} = A\chi + \Gamma(\chi), \tag{18}$$

where A is the system matrix of the linearized system, for example, $A := \nabla f(0)$, and the elements of the vector $\Gamma(\chi)$ contain (second or higher order) products of the components of χ. The proof of the claim of asymptotic stability of Proposition 1 follows, showing that A is a Hurwitz matrix.

To obtain the closed-loop dynamic behavior of χ_{13}, first notice, recognizing the Hamiltonian structure [31] of the dq system (7), that it can be written in the form

$$\dot{x} = F(x)\frac{\partial H(x)}{\partial x} + \begin{bmatrix} v \\ -\tau_L \end{bmatrix} \tag{19}$$

with

$$x := \begin{bmatrix} Li_{12} \\ J\omega \end{bmatrix} = \begin{bmatrix} Li_1 \\ Li_2 \\ J\omega \end{bmatrix},$$

$H(x) = \frac{1}{2}x^\top Q x$ the energy function,

$$Q = \begin{bmatrix} \frac{1}{L}I_2 & 0 \\ 0 & \frac{1}{J} \end{bmatrix}, \tag{20}$$

and the interconnection and damping matrices lumped into

$$F(x) = \begin{bmatrix} -RI_2 & -n_p\mathcal{J}\left(Li_{12} + \Phi e_1\right) \\ n_p\left(Li_{12} + \Phi e_1\right)^\top \mathcal{J}^\top & 0 \end{bmatrix}.$$

On the other hand, under the definition $\tilde{\rho}_{\alpha\beta} := \hat{\rho}_{\alpha\beta} - \rho_{\alpha\beta}$, the output-feedback controller (11) can be written as

$$v_{\alpha\beta} = \left[\tilde{\rho}_\alpha I_2 + \tilde{\rho}_\beta \mathcal{J}\right]\hat{v} + e^{\mathcal{J}\theta}\hat{v},$$

which, in dq coordinates, takes the form

$$\begin{aligned} v &= e^{-\mathcal{J}\theta}v_{\alpha\beta} \\ &= \hat{v} + e^{-\mathcal{J}\theta}\left[\tilde{\rho}_\alpha I_2 + \tilde{\rho}_\beta\mathcal{J}\right]\hat{v} \\ &= \hat{v} + \left[\hat{v}_1 I_2 + \hat{v}_2\mathcal{J}\right]\chi_{45}, \end{aligned} \tag{21}$$

where we have used the errors $\chi_{45} = e^{-\mathcal{J}\theta}\tilde{\rho}_{\alpha\beta}$, and $\hat{v}_1$ and $\hat{v}_2$ are the components of $\hat{v}$.

Some simple calculations show that

$$\hat{v} = v^{FI} + \begin{bmatrix} -\frac{L}{\Phi}\tau_L & -\frac{L}{J\Phi}\omega^* \\ 0 & \frac{r}{n_p\Phi} \end{bmatrix}\chi_{67} - \begin{bmatrix} \frac{L\chi_7}{\Phi}\left(\frac{1}{J}\chi_3 + \chi_6\right) \\ 0 \end{bmatrix}$$

with the full-information control given by

$$v^{FI} = (R-r)i_{12} + \begin{bmatrix} -\frac{L}{J\Phi}\tau_L\omega \\ n_p\Phi\omega^\star + \frac{r}{n_p\Phi}\tau_L \end{bmatrix}, \tag{22}$$

DOI: 10.1002/rnc

which, using the definition of χ_3, can be decomposed as

$$v^{FI} = (R-r)i_{12} + \begin{bmatrix} -\frac{L}{J\Phi}\tau_L\omega^* \\ \frac{n_p\Phi}{J}\omega^* + \frac{r}{n_p\Phi}\tau_L \end{bmatrix} + \begin{bmatrix} -\frac{L}{J\Phi}\tau_L\chi_3 \\ 0 \end{bmatrix}.$$

In addition, the second term of the control law (21) can be expanded as

$$[\hat{v}_1 I_2 + \hat{v}_2 \mathcal{J}]\,\chi_{45} = \begin{bmatrix} -\frac{L}{J\Phi}\tau_L\omega^* & -(R-r)i_2^* - \frac{n_p\Phi}{J}\omega^* - \frac{r}{n_p\Phi}\tau_L \\ (R-r)i_2^* + \frac{n_p\Phi}{J}\omega^* + \frac{r}{n_p\Phi}\tau_L & -\frac{L}{J\Phi}\tau_L\omega^* \end{bmatrix}\chi_{45} + \Gamma_{13}(\chi)$$

for some $\Gamma_{13}(\chi)$ that satisfies $\nabla\Gamma_{13}(0) = 0$.

Using all the aforementioned expressions to define v, and replacing in (19), yields

$$\dot{\chi}_{13} = A_{11}\chi_{13} + A_{12}\chi_{45} + A_{13}\chi_{67} + \Gamma_{13}(\chi), \tag{23}$$

where

$$A_{11} = \begin{bmatrix} -\frac{r}{L} & \frac{n_p}{J}\omega^* & 0 \\ -\frac{n_p}{J}\omega^* & -\frac{r}{L} & -\frac{n_p\Phi}{J} \\ 0 & \frac{n_p\Phi}{L} & 0 \end{bmatrix} \tag{24}$$

$$A_{12} = \begin{bmatrix} -\frac{L}{J\Phi}\tau_L\omega^* & -(R-r)i_2^* - \frac{n_p\Phi}{J}\omega^* - \frac{r}{n_p\Phi}\tau_L \\ (R-r)i_2^* + \frac{n_p\Phi}{J}\omega^* + \frac{r}{n_p\Phi}\tau_L & -\frac{L}{J\Phi}\tau_L\omega^* \\ 0 & 0 \end{bmatrix}$$

$$A_{13} = \begin{bmatrix} -\frac{L}{\Phi}\tau_L & -\frac{L}{J\Phi}\omega^* \\ 0 & \frac{r}{n_p\Phi} \\ 0 & 0 \end{bmatrix} \tag{25}$$

At this point, it is important to remark that matrix A_{11} is Hurwitz. This can be proved by noticing that its characteristic polynomial is of the form $s^3 + c_1 s^2 + c_2 s + c_3$, with the coefficients $c_i > 0$, and verifying $c_1 c_2 > c_3$ which, via a simple Routh–Hurwitz test, proves is the necessary and sufficient condition for stability of this matrix.

Before proceeding with the fourth and fifth components, χ_{45}, of the error vector (10), a useful preliminary step is related with the description of the position observer (12) in terms of $\rho_{\alpha\beta}$. To obtain this, recall that in PMSMs the stator flux, λ, is related with the currents and voltages via [28]

$$\lambda = L i_{\alpha\beta} + \Phi\rho_{\alpha\beta}. \tag{26}$$

From this equation, it is possible to define the estimate (13), leading to $\tilde{\lambda} = \Phi\tilde{\rho}_{\alpha\beta}$ where $\tilde{\lambda} = \hat{\lambda} - \lambda$. On the other hand, from the structure of the proposed flux observer (12), the observation error $\tilde{\lambda}$ can be described by

$$\dot{\tilde{\lambda}} = -\gamma\left[|\tilde{\lambda}|^2 + 2\Phi\tilde{\lambda}^\top\rho_{\alpha\beta}(t)\right]\left[\tilde{\lambda} + \Phi\rho_{\alpha\beta}(t)\right]. \tag{27}$$

Combining these expressions, it is obtained that

$$\dot{\tilde{\lambda}} = -\gamma\Phi^3\left(|\tilde{\rho}_{\alpha\beta}|^2 + 2\tilde{\rho}_{\alpha\beta}^\top\rho_{\alpha\beta}\right)\left(\tilde{\rho}_{\alpha\beta} + \rho_{\alpha\beta}\right)$$

implying that the estimation error $\tilde{\rho}_{\alpha\beta}$ satisfies

$$\dot{\tilde{\rho}}_{\alpha\beta} = -\gamma\Phi^2\left(|\tilde{\rho}_{\alpha\beta}|^2 + 2\tilde{\rho}_{\alpha\beta}^\top\rho_{\alpha\beta}\right)\left(\tilde{\rho}_{\alpha\beta} + \rho_{\alpha\beta}\right). \tag{28}$$

DOI: 10.1002/rnc

Moreover, noticing that

$$|\tilde{\rho}_{\alpha\beta}|^2 + 2\tilde{\rho}_{\alpha\beta}^\top \rho_{\alpha\beta} = |\hat{\rho}_{\alpha\beta}|^2 - 1,$$

whereas

$$\dot{\tilde{\rho}}_{\alpha\beta} = \dot{\hat{\rho}}_{\alpha\beta} - n_p \omega \mathcal{J} \rho_{\alpha\beta},$$

from (28) the observer (12) may be written as

$$\dot{\hat{\rho}}_{\alpha\beta} = -\gamma \Phi^2 \left(|\hat{\rho}_{\alpha\beta}|^2 - 1\right) \hat{\rho}_{\alpha\beta} + n_p \omega \mathcal{J} \rho_{\alpha\beta}. \tag{29}$$

Consider now the time derivative of $\chi_{45} = e^{-\mathcal{J}\theta}\tilde{\rho}_{\alpha\beta}$ given by

$$\dot{\chi}_{45} = -\frac{n_p}{J}\omega \mathcal{J} \chi_{45} + e^{-\mathcal{J}\theta}\dot{\tilde{\rho}}_{\alpha\beta}.$$

Using the facts that $|\tilde{\rho}_{\alpha\beta}| = |\chi_{45}|$ and that $e^{-\mathcal{J}\theta}\rho_{\alpha\beta} = e_1$, defined in (8), it is possible to write (28) as

$$\dot{\tilde{\rho}}_{\alpha\beta} = -\gamma \Phi^2 \left(|\chi_{45}|^2 + 2\chi_{45}^\top e_1\right) e^{\mathcal{J}\theta} \left(\chi_{45} + e_1\right).$$

Replacing the latter in the expression above yields

$$\dot{\chi}_{45} = -\left[\frac{n_p}{J}(\omega^\star + \chi_3)\mathcal{J} + \gamma \Phi^2 \left(|\chi_{45}|^2 + 2\chi_4\right)\right] \chi_{45} - \gamma \Phi^2 \left(|\chi_{45}|^2 + 2\chi_4\right) e_1,$$

which can be written as

$$\dot{\chi}_{45} = A_{22}\chi_{45} + \Gamma_{45}(\chi) \tag{30}$$

with

$$A_{22} = \begin{bmatrix} -2\gamma\Phi^2 & \frac{n_p}{J}\omega^\star \\ -\frac{n_p}{J}\omega^\star & 0 \end{bmatrix} \tag{31}$$

and $\Gamma_{45}(\chi)$ is such that $\nabla\Gamma_{45}(0) = 0$. Moreover, it can be trivially proved, computing its characteristic polynomial, that, for all $\omega^\star \neq 0$, A_{22} is Hurwitz.

The final component of (17) is related with the closed-loop behavior of χ_{67}. To obtain their dynamics, consider, from the observer (15), that the estimates for speed and load torque are given by

$$\begin{bmatrix} \hat{\omega} \\ \hat{\tau}_L \end{bmatrix} = \xi + \begin{bmatrix} a_1 \\ -a_2 \end{bmatrix} \mathcal{A}\left(\frac{\hat{\rho}_\beta}{\hat{\rho}_\alpha}\right) \tag{32}$$

leading to

$$\chi_{67} = \begin{bmatrix} \hat{\omega} - \omega \\ \hat{\tau}_L - \tau_L \end{bmatrix} = \xi - \begin{bmatrix} \omega \\ \tau_L \end{bmatrix} + \begin{bmatrix} a_1 \\ -a_2 \end{bmatrix} \mathcal{A}\left(\frac{\hat{\rho}_\beta}{\hat{\rho}_\alpha}\right).$$

Taking the time derivative of this equation yields

$$\dot{\chi}_{67} = \dot{\xi} - \begin{bmatrix} \dot{\omega} \\ \dot{\tau}_L \end{bmatrix} + \begin{bmatrix} a_1 \\ -a_2 \end{bmatrix} \frac{1}{|\hat{\rho}_{\alpha\beta}|^2} \hat{\rho}_{\alpha\beta}^T \mathcal{J} \dot{\hat{\rho}}_{\alpha\beta}$$

under the assumed structure for the operator $\mathcal{A}(\cdot)$.

On the other hand, the mechanical (3) and the position observer (29) can be written in the 'perturbed' form as

$$\begin{aligned} J\dot{\omega} &= n_p \Phi i_{\alpha\beta}^\top \mathcal{J} \hat{\rho}_{\alpha\beta} - \tau_L - \left(n_p \Phi i_{\alpha\beta}^\top \mathcal{J} \tilde{\rho}_{\alpha\beta}\right) \\ \dot{\hat{\rho}}_{\alpha\beta} &= -\gamma \Phi^2 \left(|\hat{\rho}_{\alpha\beta}|^2 - 1\right) \hat{\rho}_{\alpha\beta} + n_p \omega \mathcal{J} \hat{\rho}_{\alpha\beta} - (n_p \omega \mathcal{J} \tilde{\rho}_{\alpha\beta}). \end{aligned} \tag{33}$$

DOI: 10.1002/rnc

Replacing these equations, together with $\dot{\tau}_L = 0$, in the aforementioned expression leads to

$$\dot{\chi}_{67} = \begin{bmatrix} -n_p a_1 & -\frac{1}{J} \\ n_p a_2 & 0 \end{bmatrix} \chi_{67} - \frac{n_p \omega}{|\hat{\rho}_{\alpha\beta}|^2} \begin{bmatrix} a_1 \\ -a_2 \end{bmatrix} \hat{\rho}_{\alpha\beta}^\top \tilde{\rho}_{\alpha\beta} + \begin{bmatrix} \frac{n_p \Phi}{J} i_{\alpha\beta}^\top \mathcal{J} \tilde{\rho}_{\alpha\beta} \\ 0 \end{bmatrix}, \tag{34}$$

where

$$\begin{aligned} i_{\alpha\beta}^\top \mathcal{J} \tilde{\rho}_{\alpha\beta} &= \frac{1}{L} i_{12}^\top e^{\mathcal{J}\theta} \mathcal{J} \tilde{\rho}_{\alpha\beta} \\ &= \frac{1}{L} i_{12}^\top \mathcal{J} \chi_{45} \\ &= \frac{1}{L} \chi_{12}^\top \mathcal{J} \chi_{45} + \frac{1}{L} \left(i_{12}^\star\right)^\top \mathcal{J} \chi_{45}, \end{aligned} \tag{35}$$

whereas

$$\begin{aligned} \frac{n_p \omega}{|\hat{\rho}_{\alpha\beta}|^2} \hat{\rho}_{\alpha\beta}^\top \tilde{\rho}_{\alpha\beta} &= \frac{n_p}{J} \frac{\omega}{|\hat{\rho}_{\alpha\beta}|^2} \hat{\rho}^\top \chi_{45} \\ &= \frac{n_p}{J} \frac{\omega}{|\hat{\rho}_{\alpha\beta}|^2} \left(\chi_{45} + e_1\right)^\top \chi_{45} \\ &= \frac{n_p}{J} \frac{\omega}{|\hat{\rho}_{\alpha\beta}|^2} \left(|\chi_{45}|^2 + \chi_4\right). \end{aligned}$$

If the denominator of the last right-hand term is expanded as

$$|\hat{\rho}_{\alpha\beta}|^2 = |\chi_{45} + e_1|^2 = |\chi_{45}|^2 + 2\chi_4 + 1,$$

and it is noticed that

$$\frac{|\chi_{45}|^2 + \chi_4}{|\chi_{45}|^2 + 2\chi_4 + 1} = \chi_4 + \Omega\left(|\chi|^2\right),$$

where $\Omega(|\chi|^2)$ contains term of order higher or equal to $|\chi|^2$, then

$$\frac{n_p \omega}{|\hat{\rho}_{\alpha\beta}|^2} \hat{\rho}_{\alpha\beta}^\top \tilde{\rho}_{\alpha\beta} = \frac{n_p}{J} \left(\omega^\star + \chi_3\right) \chi_4 + \Omega\left(|\chi|^2\right), \tag{36}$$

from which, considering that $i_1^\star = 0$, it is possible to write

$$\dot{\chi}_{67} = A_{32} \chi_{45} + A_{33} \chi_{67} + \Gamma_{67}(\chi), \tag{37}$$

where

$$A_{32} = \begin{bmatrix} -\frac{n_p}{J} \left(a_1 \omega^\star - \frac{\Phi i_2^\star}{L}\right) & 0 \\ \frac{n_p}{J} a_2 \omega^\star & 0 \end{bmatrix}, \tag{38}$$

A_{33} as in (16) and $\Gamma_{67}(\chi)$ is such that $\nabla\Gamma_{67}(0) = 0$. In this case, the stability properties of matrix A_{33} are immediately recognized.

Once expressions (23), (30), and (37) have been derived, the final part of the proof follows combining these results to obtain that the error vector χ satisfies a differential equation of the form (18) where

$$A = \begin{bmatrix} A_{11} & A_{12} & A_{13} \\ 0 & A_{22} & 0 \\ 0 & A_{32} & A_{33} \end{bmatrix}, \quad \Gamma(\chi) = \begin{bmatrix} \Gamma_{13}(\chi) \\ \Gamma_{45}(\chi) \\ \Gamma_{67}(\chi) \end{bmatrix}.$$

Recalling that $\nabla\Gamma(0) = 0$, it only remains to prove that A is Hurwitz. For, we notice that A is similar to a block triangular Hurwitz matrix. More precisely, with

$$T = \begin{bmatrix} I_3 & 0 & 0 \\ 0 & 0 & I_2 \\ 0 & I_2 & 0 \end{bmatrix},$$

DOI: 10.1002/rnc

we get

$$TAT^{-1} = \begin{bmatrix} A_{11} & A_{12} & A_{13} \\ 0 & A_{33} & A_{32} \\ 0 & 0 & A_{22} \end{bmatrix},$$

which is Hurwitz because A_{11}, A_{22}, and A_{33} are Hurwitz matrices, completing the proof. □

Remark 7

An interesting feature of the closed-loop system (17) that allowed to conclude the aforementioned stability properties is its independent structure with respect to the cyclic coordinates $\rho_{\alpha\beta}$. This is due to the choice of carrying the analysis out by mixing dq and $\alpha\beta$ coordinates in the error vector (10).

4. ADDITIONAL STABILITY PROPERTIES

Proposition 1 proves that the proposed sensorless controller is exponentially stable, but only locally, and no explicit evaluation of the domain of attraction is given. On the other hand, the numerical and experimental evaluation reported in Section 5 shows a remarkable behavior that leads us to believe that the domain of attraction of the equilibrium is, actually, quite large. To further substantiate this conjecture, we prove in this section that each of the components of the overall scheme, for example, the controller (11)–(16), when analyzed separately, exhibit very strong *global* stability properties.

Another objective of this section is to clarify the procedure used in the derivation of the proposed overall controller, which relied on the application of the systematic design methodologies of IDA-PBC and I&I.

4.1. Full information control

The full information (state-feedback) version of the controller (11) is presented in (22). This scheme is obtained, in a similar way as in [15, 16], by applying the IDA-PBC design methodology.

The objective of IDA-PBC is to find a state-feedback control law $v = v(x)$ that assigns to the closed-loop a desired energy function, say $H_d(x)$, which satisfies $x^\star = \arg\min H_d(x)$. This is achieved modifying the interconnection and damping matrices, endowing the closed-loop with the port-Hamiltonian form

$$\dot{x} = F_d(x)\nabla H_d(x), \tag{39}$$

where $F_d(x) + F_d^\top(x) \leqslant 0$. This ensures stability of the equilibrium $x^\star$ with Lyapunov function $H_d(x)$. Under some standard detectability assumptions, for example, Lemma 3.8 of [31], the equilibrium is shown to be asymptotically stable.

In the particular case of the PMSM model (7), it is possible to exploit its Hamiltonian structure, given in (19), to proposed a desired closed-loop energy function as the quadratic in the errors form

$$H_d(\chi_{13}) = \frac{1}{2}\chi_{13}^\top Q\chi_{13},$$

where Q is as in (20). Under this definition and equating the right hand sides of (19) and (39), it is possible to show that the desired port-Hamiltonian form (39) is achieved under the control law (22) with

$$F_d(x) = \begin{bmatrix} -r & \frac{Ln_p}{J}x_3 & 0 \\ -\frac{Ln_p}{J}x_3 & -r & -n_p\Phi \\ 0 & n_p\Phi & 0 \end{bmatrix}, \tag{40}$$

proving, hence, that the equilibrium

$$x^\star = \begin{bmatrix} 0 \\ \frac{L}{n_p\Phi}\tau_L \\ J\omega^\star \end{bmatrix}$$

DOI: 10.1002/rnc

is stable. Moreover, noting that

$$\dot{H}_d = -\frac{r}{L^2}|\chi_{12}|^2$$

and that $|\chi_{12}|^2$ is a zero-state detectable output for the closed-loop system, it can be concluded that $x^\star$ is rendered *globally asymptotically stable*.

4.2. *Position observer of* [9]

The observer presented in (12) was first reported in [9]. It was developed taking advantage of the fact that $\dot{\lambda}$, given by

$$\dot{\lambda} = -Ri_{\alpha\beta} + v_{\alpha\beta},$$

is measurable and that the vector function $\eta(\lambda) = \lambda - Li_{\alpha\beta}$ satisfies $|\eta(\lambda)| = \Phi$. In [9], it is shown that (27) enjoys the following remarkable stability properties.

P1. *(Global stability)* For arbitrary speeds, the disk

$$\left\{\tilde{\lambda} \in \mathbb{R}^2 \,|\, |\tilde{\lambda}| \leqslant 2\Phi\right\}$$

is globally attractive. This means, that all trajectories of (27) will converge to this disk.

P2. *(Exponential stability under persistent excitation)* The zero equilibrium of (27) is exponentially stable if there exists constants $T, \Delta > 0$ such that

$$\frac{1}{T}\int_t^{t+T} \omega^2(s)\mathrm{d}s \geqslant \Delta,$$

for all $t \geqslant 0$.

P3. *(Constant non-zero speed)* If the speed is constant and satisfies

$$|\omega| > \frac{1}{4}\gamma\Phi^2,$$

then the origin is the unique equilibrium of (27), and it is globally asymptotically stable.[‖]

Remark 8
Property P3 is trivially satisfied for an observer that generates directly an estimate of θ, say $\hat{\theta}$, and then define

$$\hat{\lambda} := \begin{bmatrix} \cos\left(\hat{\theta}\right) \\ \sin\left(\hat{\theta}\right) \end{bmatrix}.$$

This is because the largest distance between any two points on the unit disk is 2. It is not trivial in our case because the observer estimates λ and not θ.

4.3. *Speed and load torque observer*

The observer (15) introduced to estimate the unmeasurable variables ω and τ_L was designed following the I&I methodology [12]. For its construction, it is assumed that the motor position is known, that is, in (33), it is considered that $\tilde{\rho}_{\alpha\beta} = 0$, and the objective is to render attractive and invariant the manifold

$$\mathcal{M} := \left\{\left(\xi, \omega, \hat{\rho}_{\alpha\beta}\right) : \xi - \begin{bmatrix} \omega \\ \tau_L \end{bmatrix} + \zeta\left(\hat{\rho}_{\alpha\beta}\right) = 0\right\} \subset \mathbb{R}^5, \tag{41}$$

[‖]Notice the presence of the free adaptation gain γ on the lower bound.

DOI: 10.1002/rnc

for a suitable mapping $\zeta\left(\hat{\rho}_{\alpha\beta}\right)$, which is equivalent to prove that the off-the-manifold coordinate

$$\chi_{67} := \xi - \begin{bmatrix} \omega \\ \tau_L \end{bmatrix} + \zeta\left(\hat{\rho}_{\alpha\beta}\right),$$

is such that:

- $\chi_{67}(0) = 0 \Rightarrow \chi_{67}(t) = 0$, for all $t \geqslant 0$ (invariance);
- $\chi_{67}(t)$ asymptotically (*exponentially*) converges to zero (attractivity).

To achieve this property, it is considered the dynamics of χ_{67} along the trajectories (33), with $\tilde{\rho}_{\alpha\beta} = 0$, to obtain

$$\dot{\chi}_{67} = \dot{\xi} - \nabla\zeta\left[\gamma\Phi^2\left(|\hat{\rho}_{\alpha\beta}|^2 - 1\right)\hat{\rho}_{\alpha\beta} - n_p\omega\mathcal{J}\hat{\rho}_{\alpha\beta}\right] + \begin{bmatrix} \frac{\tau_L}{J} - \frac{n_p\Phi}{J} i_{\alpha\beta}^{\top}\mathcal{J}\hat{\rho}_{\alpha\beta} \\ 0 \end{bmatrix}.$$

Hence, if the structure for the observer (15) is replaced together with

$$\zeta(\hat{\rho}_{\alpha\beta}) = \begin{bmatrix} a_1 \\ -a_2 \end{bmatrix} \arctan\left(\frac{\hat{\rho}_\beta}{\hat{\rho}_\alpha}\right), \tag{42}$$

it is obtained that

$$\dot{\chi}_{67} = A_{33}\chi_{67},$$

establishing that for some $\alpha > 0$ and for all initial conditions $(\omega(0), \xi(0)) \in \mathbb{R} \times \mathbb{R}^2$,

$$\lim_{t\to\infty} e^{\alpha t}\left\|\begin{bmatrix} \hat{\omega}(t) - \omega(t) \\ \hat{\tau}_L(t) - \tau_L \end{bmatrix}\right\| = 0. \tag{43}$$

That is, (15) is a *globally exponentially* convergent speed and load torque observer when the motor position is known.

Remark 9

Notice that if the arctan function that appears in (42) is directly used, instead of the operator $\mathcal{A}$, in the observer (15), some Dirac delta functions might appear in the speed estimation and the error dynamics. To explain this phenomenon, consider the case of (constant) regulation of the motor speed and assume that $\hat{\rho}_{\alpha\beta}(t) \equiv \rho_{\alpha\beta}(t)$. Then, in view of (42), we have that $\zeta(\hat{\rho}_{\alpha\beta}(t)) \equiv \theta(t) = \omega^\star t (\mathrm{mod}\,\pi)$, which is a periodic function defined on the set $(-\pi, \pi)$. As shown in Figure 1

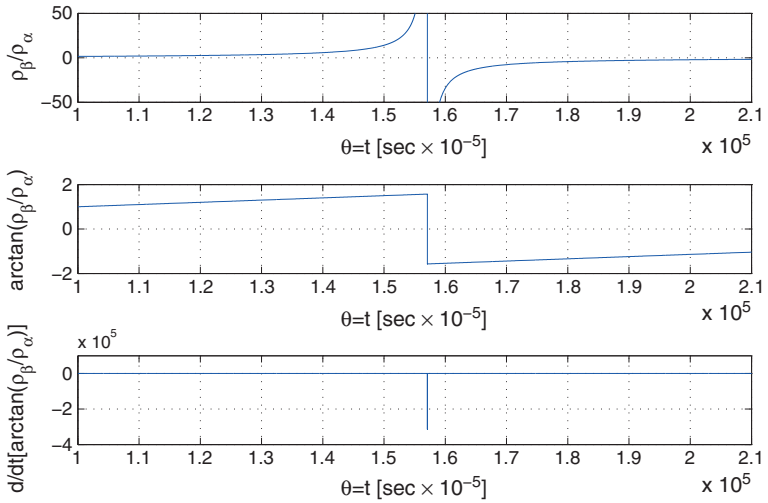

Figure 1. Behavior of $\frac{\rho_\beta}{\rho_\alpha}$, $\arctan\left(\frac{\rho_\beta}{\rho_\alpha}\right)$ and $\frac{\mathrm{d}}{\mathrm{d}t}\left(\arctan\left(\frac{\rho_\beta}{\rho_\alpha}\right)\right)$ when $\theta(t) = t\,(\mathrm{mod}\,\pi)$.

DOI: 10.1002/rnc

(when $\omega^\star = 1$), in this scenario, the arctan jumps instantaneously from the value $\frac{\pi}{2}$ to the value $\frac{-\pi}{2}$ inducing a train of Dirac delta functions, $\delta_T(t)$, in the derivative of arctan. This term propagates, through $\dot{\zeta}(\rho_{\alpha\beta})$, into the error dynamics that now reads as[**]

$$\dot{\chi}_{67} = \begin{bmatrix} -n_p a_1 & -\frac{1}{J} \\ n_p a_2 & 0 \end{bmatrix} \chi_{67} + \begin{bmatrix} a_1 \\ -a_2 \end{bmatrix} \delta_T.$$

As illustrated in the simulations of Section 5, this undesirable effect is removed using instead the operator $\mathcal{A}$ defined in Appendix A.

5. SIMULATION AND EXPERIMENTAL RESULTS

The usefulness of the proposed control scheme was evaluated through numerical simulations and experiments. For the simulations, the considered motor parameters were $L = 0.0038H$, $R = 0.225\Omega$, $\Phi = 0.17Wb$, $n_p = 3$, and $J = 0.012kg.m^2$, which correspond to a ($1Kw$ rated power, $1N.m$ rated torque) motor included in an experimental setup located in the *Laboratoire de Genie Electrique de Paris*, where the experiments were carried out.

5.1. Simulation results

Three types of simulations were developed; the first was devoted to illustrate the performance under nominal (ideal) conditions, where the motor parameters are known, whereas the second was intended to exhibit the operation under several cases of parametric uncertainty. Finally, we carried out a third set of simulations to compare the performance of the proposed scheme with one proposed in the drives community, namely the one reported in [4]. The signal profiles and the parameter variations were taken from the benchmark proposed by the French Working Group *Commande des Entraînements Electriques* and are as follows.[††]

- The desired speed started in zero, increasing with a slope of 50 $\frac{\text{rpm}}{\text{s}}$ until reaching a value of 50 rpm at $t = 1$ s. This value was kept constant until $t = 3$ s when its value was increased again, this time with a slope of 35 $\frac{\text{rpm}}{\text{s}}$, to achieve a value of 120 rpm during 2 s, to be decreased (with a slope of 60 $\frac{\text{rpm}}{\text{s}}$, *remaining at zero* for the rest of the simulation (whose total length was 10 s).
- The applied load torque was switched between 0 Nm and 1 Nm. It was considered an operation without load torque from the starting time to $t = 1$ s and from $t = 2.5$ s to $t = 5$ s, whereas in the rest of the simulation its value was equal to 1 Nm.

In order to evaluate the scheme under stringent conditions, the motor was at standstill at the beginning of the simulations. Hence, the initial conditions for both currents and speed as well as the initial values for the estimated speed and load torque were set to zero; on the other hand, to avoid singularities, the initial conditions of the position observer were set as $\hat{\rho}_\alpha(0) = \Phi$ and $\hat{\rho}_\beta(0) = 0$.

The tuning parameters of the control scheme were chosen as $\gamma = 5000$, for the $\rho_{\alpha\beta}$ observer, and $a_1 = 20$, $a_2 = 6$, for the speed-load torque observer. In both cases, the selection was taken to obtain a better response of the closed-loop system under parametric uncertainty operation. The high value assigned to the gain γ is due to the high sensitivity exhibited by the position observer with respect to the stator resistance R.

Figures 2–4 show the behavior of the closed-loop system under nominal operation. In Figure 2, the behavior of the motor speed and the load torque is given. In the top of this figure, both the actual and the desired speeds are shown. Here, it can be noticed that, as predicted by the theory, when the desired speed is constant, the achieved performance is remarkable. Moreover, when the speed reference is time-varying the speed error still remains within reasonable values. In the bottom of the same figure, the actual load torque and its estimate are presented.

[**]The aforementioned expression shows that, away from the isolated points where the δ-functions appear, the observer error exponentially converges to zero.

[††]The complete evaluation procedure can be consulted in http://www2.irccyn.ec-nantes.fr/CE2/.

DOI: 10.1002/rnc

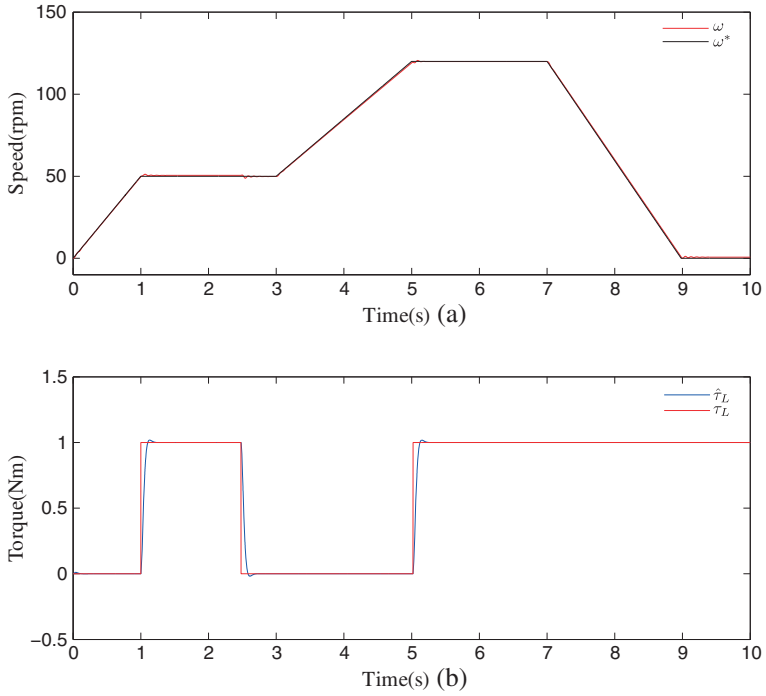

Figure 2. Reference and actual speed (top) and load torque and its estimate (bottom) in nominal operation.

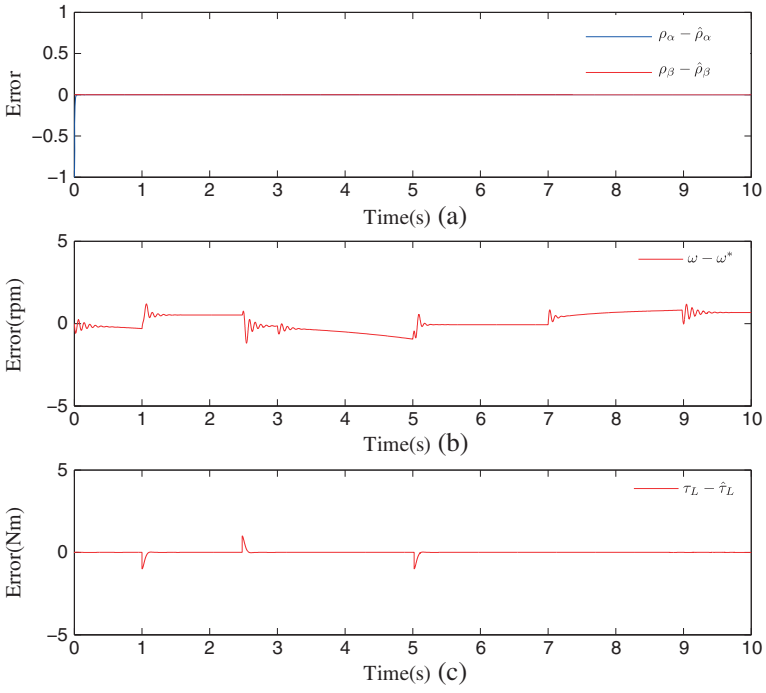

Figure 3. Observer and speed tracking errors in nominal operation.

In Figure 3, the observation errors corresponding to the position and the speed-load toque observers are presented. As can be observed, in both cases their magnitudes are negligible, even in the presence of changes in the load torque perturbation and under time-varying speed references. This picture is complemented with the tracking speed error, which is included to illustrate how the control objective is achieved under constant speed references and remains within reasonable values

DOI: 10.1002/rnc

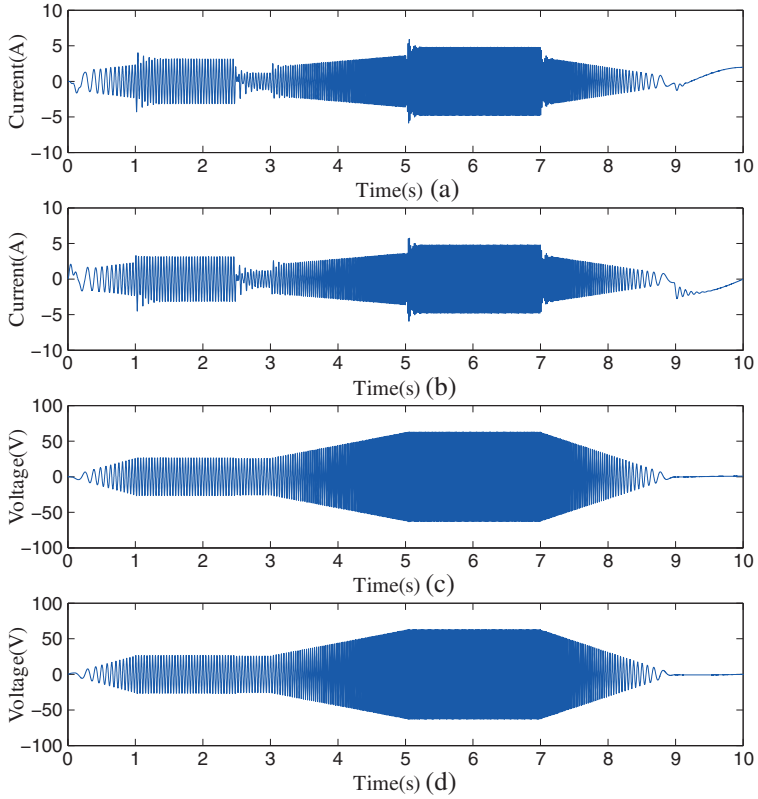

Figure 4. Stator currents and voltages in nominal operation.

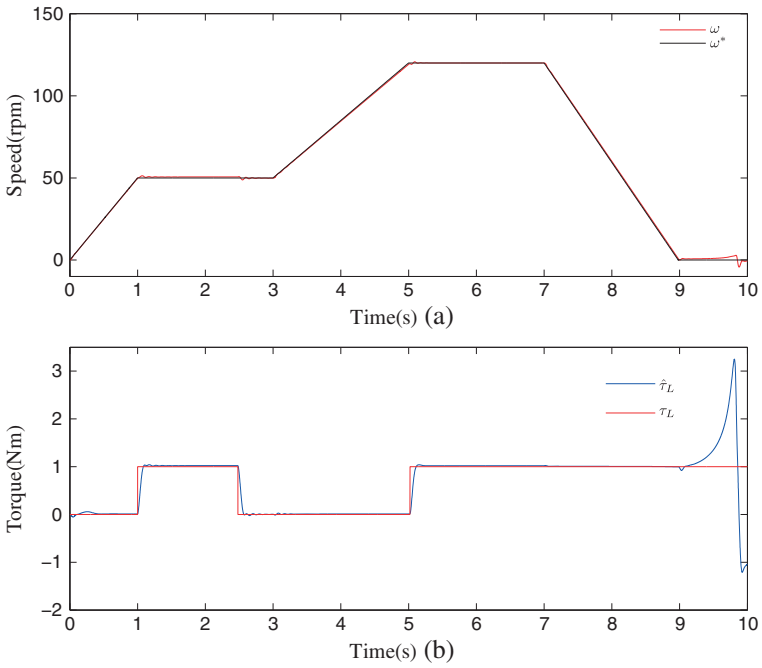

Figure 5. Reference and actual speed (top) and load torque and its estimate (bottom) with a 50% error of the stator resistance.

DOI: 10.1002/rnc

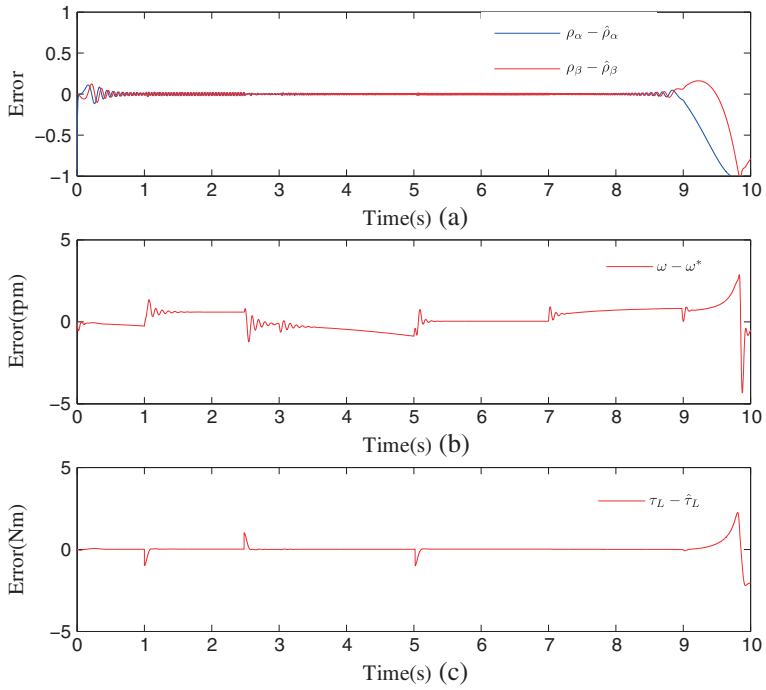

Figure 6. Observer and speed tracking errors with a 50% error of the stator resistance.

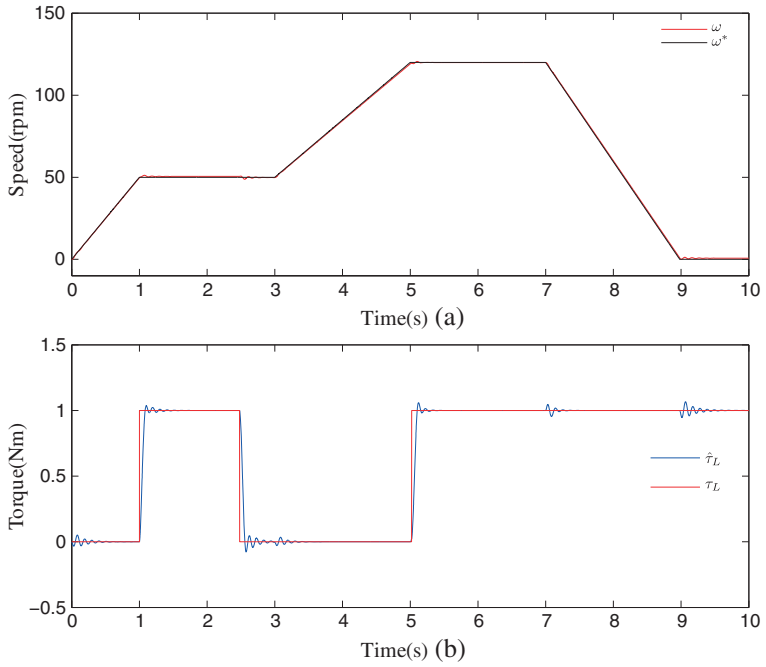

Figure 7. Reference and actual speed (top) and load torque and its estimate (bottom) with a 50% increase of the stator inductance.

under time-varying references. In Figure 4, the stator currents and voltages are given; it can be noticed that the bounds on these variables correspond to a practical operation.

To test the robustness of the controller, Figures 5–10 depict the behavior of the proposed controller under parametric uncertainty. In all these cases, only the speed, load torque, and observer errors

DOI: 10.1002/rnc

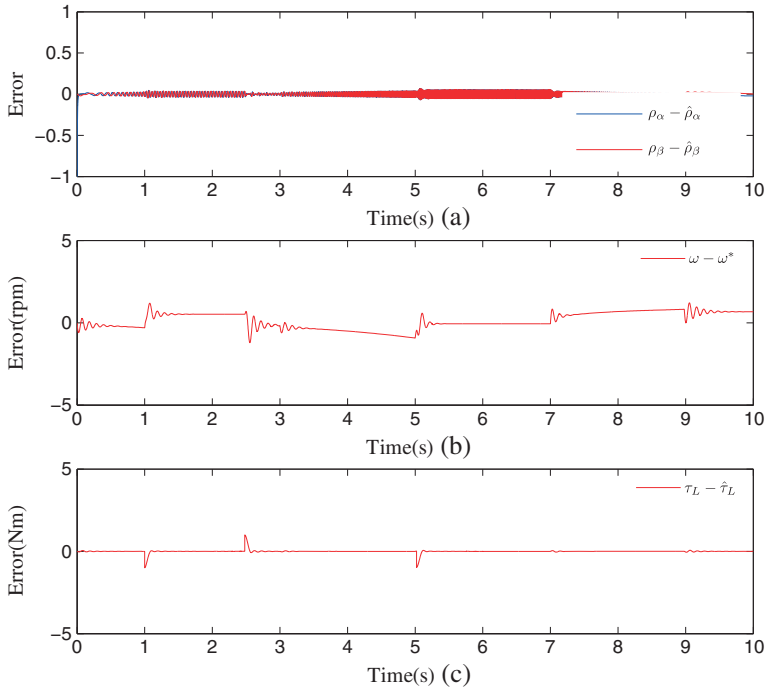

Figure 8. Observer and speed tracking errors with a 50% increase of the stator inductance.

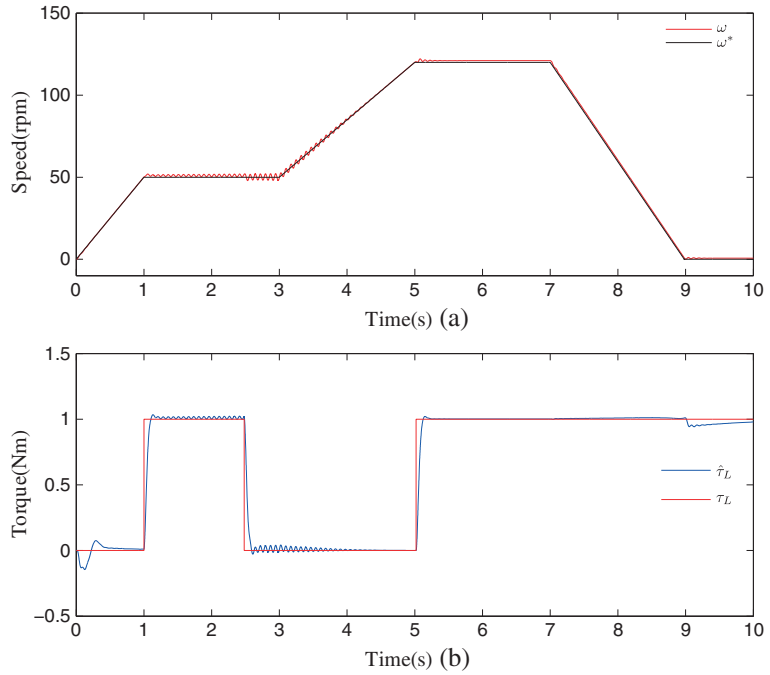

Figure 9. Reference and actual speed (top) and load torque and its estimate (bottom) with a 15% increase of the field flux.

behavior are illustrated because both stator currents and voltages remained within practical limits. In addition, it is important to mention that the presented results correspond to the maximum parameter variations that the closed-loop could support before going into instability.

DOI: 10.1002/rnc

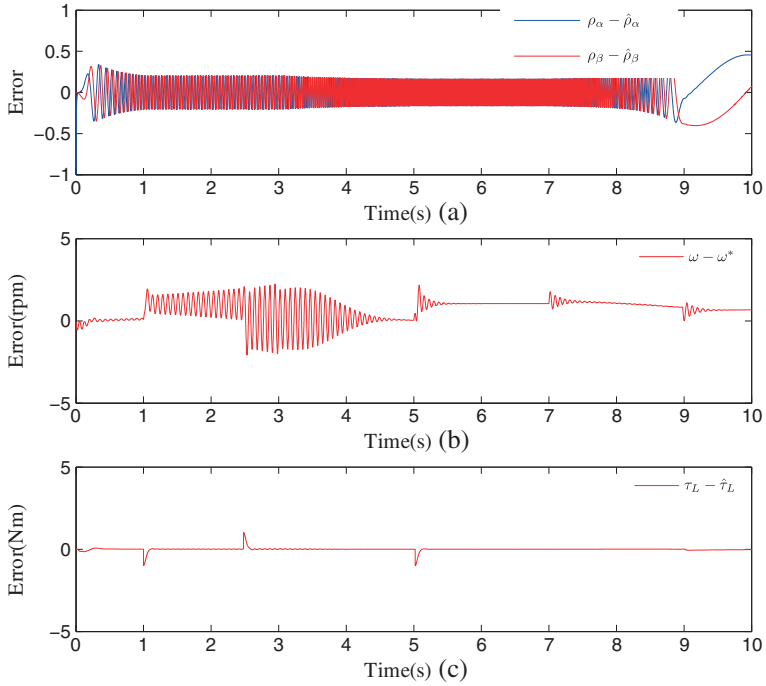

Figure 10. Observer and speed tracking errors with a 15% positive increase of the field flux.

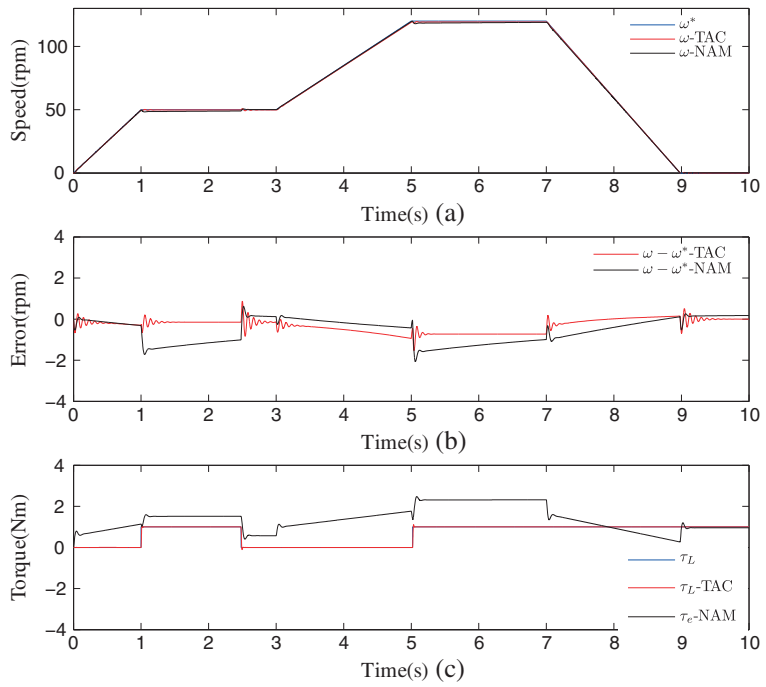

Figure 11. Comparative behavior of the proposed scheme (denoted TAC) with the one reported in [4] (denoted NAM).

Figures 5 and 6 correspond to an operation with a 50% positive variation of the stator resistance value. Despite the parametric uncertainty, the main control objective (speed tracking) is still achieved, under remarkable conditions, whereas $\omega^\star$ remains away from zero. As shown in the figures in the last portion of the simulation, the estimates diverge. This behavior is consistent with

DOI: 10.1002/rnc

the observation made in the introduction, that back-emf-based observers lose their robustness at zero speed operation. The same behavior was observed when the control scheme operates under a 50% over estimation of the inductance value, which is shown in Figures 7 and 8, and with a 15% positive variation of the constant field flux shown in Figures 9 and 10.

In [4], see also [11], the observer of [9] is used together with a phase-locked-loop like speed and load torque observer to implement an output feedback version of the classical field-oriented controller [28]. To compare the performance of our new speed and load torque observer and the proposed IDA-PBC, we show in Figure 11 the response of both schemes to the previous benchmark references. It is clear from the figure that our scheme outperforms the one in [4], both in speed regulation as well as load torque estimation.

5.2. Experimental results

Experiments were carried out to test the performance of the proposed position, speed, and load torque observers. The motor operated in closed-loop with the *full-information* IDA-PBC speed regulation scheme described in Section 4.1. Unfortunately, because of time and hardware constraints, the output feedback version has not yet been tested.

Two sets of experiments were carried out, with and without zero crossing of the speed reference. In the first case, speed is varied between 300 rpm and 600 rpm, as shown in Figure 12, where the reference, actual, and estimated speeds, as well as the estimated and actual load torques are shown. Figure 13 shows the actual and observed positions at the beginning of the trial. The behavior of the voltage and current is depicted in Figure 14.

The behavior of the system for a reference speed profile with zero crossings is shown in Figures 15–18. As seen from the figures, a transient is observed, both in the controller and the observer, while speed crosses through zero, but they recover their good behavior relatively fast.

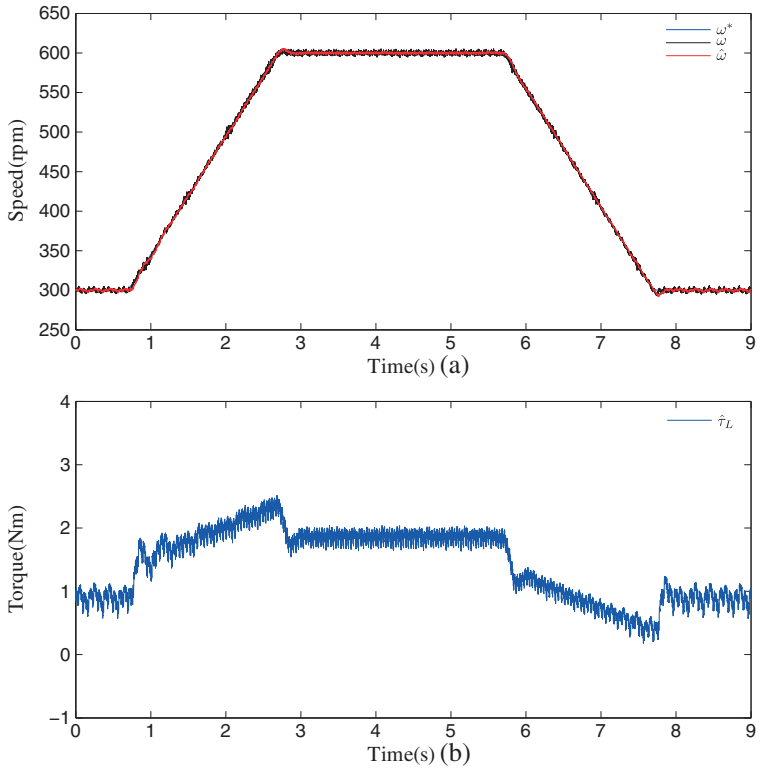

Figure 12. Reference, measured and actual speeds (top) and observed load torque (bottom) in the experimental rig.

DOI: 10.1002/rnc

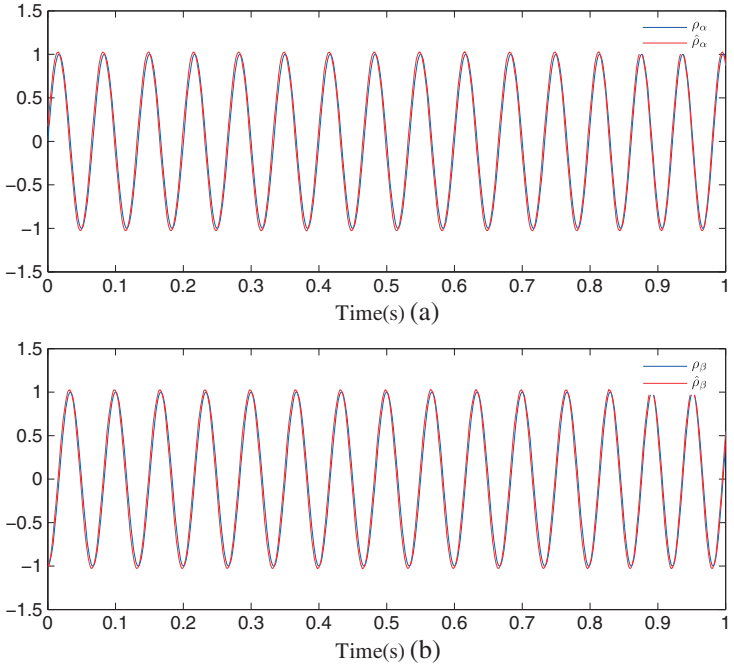

Figure 13. Measured and observed positions in the experimental rig.

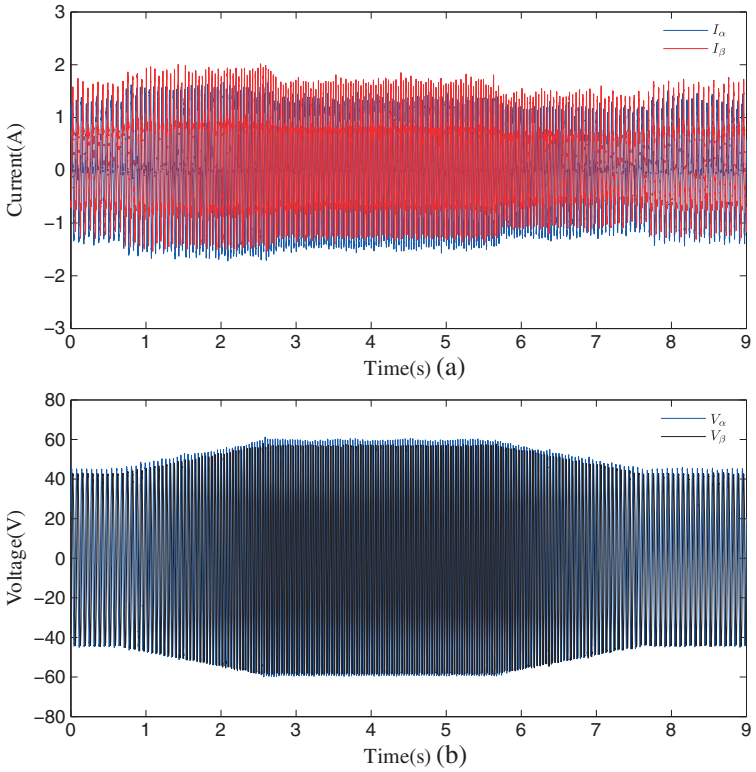

Figure 14. Currents (top) and applied voltages (bottom) in the experimental rig.

As can be noticed, the performance achieved by the state-feedback controller is remarkable. In addition, it is interesting to mention that this response was achieved with stator currents values less than 3 A and stator voltage values less than 50 V as can be shown in Figure 18.

DOI: 10.1002/rnc

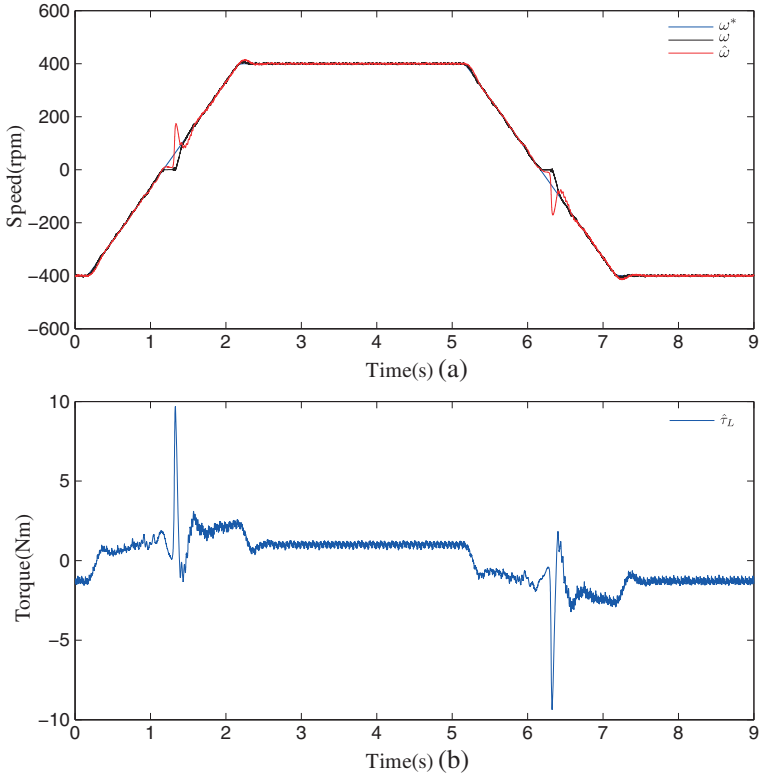

Figure 15. Measured and observed speed (top) and estimated load torque (bottom) in the experimental rig.

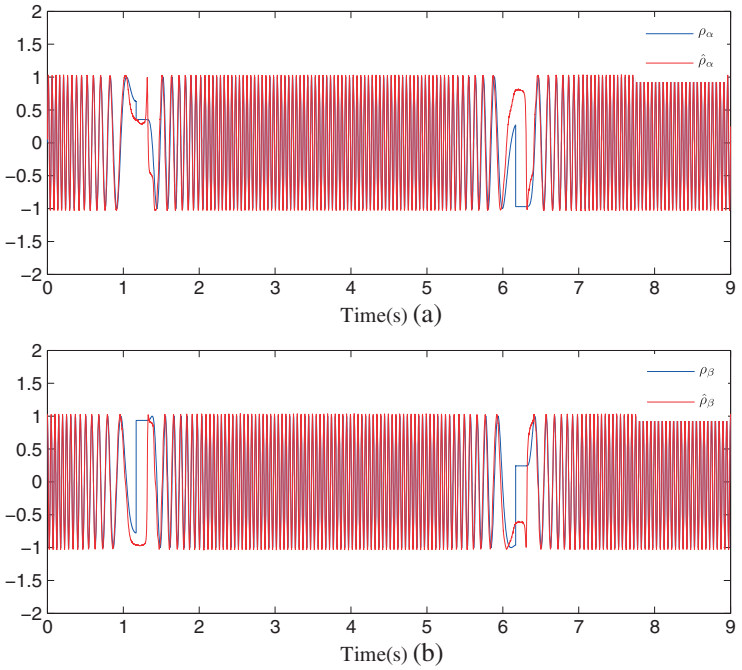

Figure 16. Position measured and observed in the experimental rig.

DOI: 10.1002/rnc

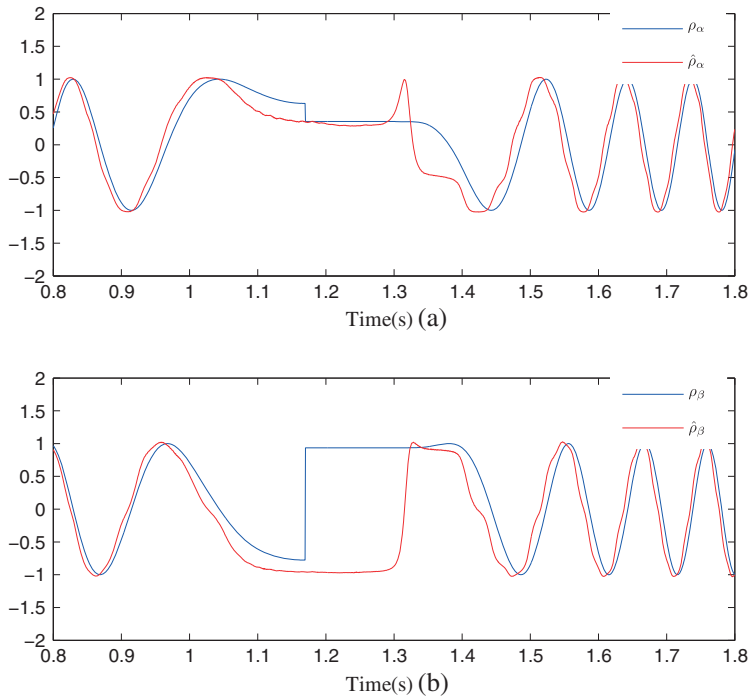

Figure 17. Estimated and measured position at zero crossing and low speed in the experimental rig.

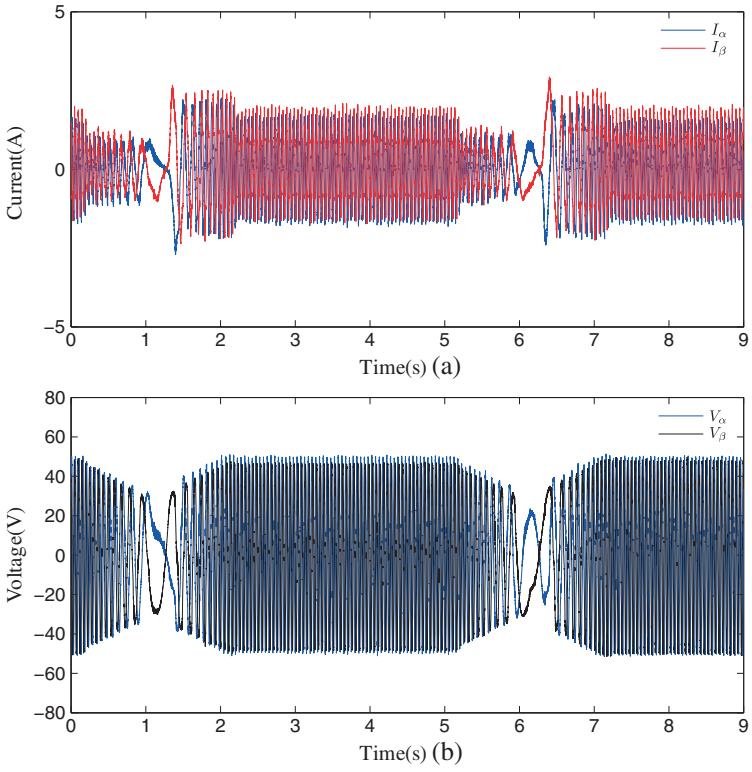

Figure 18. Current (top) and voltage (bottom) in the experimental rig.

DOI: 10.1002/rnc

6. FUTURE RESEARCH

From a theoretical viewpoint, the need to include the operator $\mathcal{A}\left(\frac{\hat{\rho}_\beta}{\hat{\rho}_\alpha}\right)$ to avoid the presence of spikes may seem unsatisfactory. However, in practice, this kind of modifications are systematically applied and widely accepted. Given the theoretical complexity of the problem, we tend to believe that the problem does not admit a 'smooth' solution. The result is presented without a detailed analysis of the effect of this operator—that is currently under investigation.

Another research line that we are currently pursuing is the establishment of a non-conservative estimate of the region of attraction of the equilibrium point. It has been observed in simulations that the estimates that are obtained with the standard Lyapunov tools are extremely conservative and provide little insight on the choice of the free parameters γ, a_1 and a_2. This research is, obviously, related with the analysis of the full-fledged nonlinear dynamics that seems a formidable task. It should be pointed out that even the (symbolic) evaluation of the roots of the vector field $f(\chi)$, to study the stability of equilibria different from the origin, is a nontrivial task.

Simulations have shown that performance is sensitive to parameter uncertainty, in particular, in the field flux. To enhance robustness, it would be interesting to incorporate an adaptation algorithm, but this task is far from trivial given the nonlinearly parameterized nature of the problem. Robustness can also be enhanced exploiting some degrees of freedom of the design that were skipped for readability. Namely, we used the simplest solution in the design of both the IDA-PBC and the I&I observers. Thus, the impact of exploiting the additional degrees of freedom on the systems performance is currently under investigation.

Some preliminary experimental results, which have confirmed the remarkable properties of the observers, have been reported here. Current research is under way to try experimentally the output-feedback controller proposed in the paper. It should be mentioned that, even though the observers were designed under the assumption of isotropic rotor, the experiments have been carried on a salient machine, confirming the robustness of the observers. It is clear that topics like the performance evaluation against unmodeled dynamics, for example, pulse width modulation switching noise, must be of principal interest.

APPENDIX A

In computer programming languages, the single argument $\arctan(u)$ function is computed in such a way that its output value e is wrapped in the set $(-\pi, \pi]$. This situation results in the existence of discontinuities because each time the output of the function e takes a value higher (lower) than π (respectively, $-\pi$), then it is assigned the value $-\pi$ (respectively, π). With the aim of avoiding these discontinuities, it is usual practice to modify the $arctan(u)$ function by including at its output an additional block whose input is e, the output of the arctan function, and its output is given by

$$y = e + 2n\pi$$

where n is a counter, initialized at zero, that is increased by 1 each time the $e > \pi$ or decreased by 1 if $e < -\pi$. From a mathematical perspective, the result is an operator, denoted as $\mathcal{A}(u)$, that has as input the argument of the arctan function and as output a continuous variable that corresponds to the unwrapped version of the original output of the arctan function.

It is clear that $\mathcal{A}(u)$ can be easily implemented in any programming language, like *C* or *Matlab*. The code for doing this considers two consecutive values of e at two consecutive sampling times, kT, $(k+1)T$ and compute its difference $dif = e[kT] - e[(k+1)T]$ in order to know if there has been a jump from π to $-\pi$ or viceversa. According to this, three different possibilities can appear

- If $dif < -2\pi$ then $n = n + 1$.
- If $dif > 2\pi$ then $n = n - 1$.
- Otherwise the value of n is not changed.

The computational loop is closed by updating the value of y and assigning $k = k + 1$.

DOI: 10.1002/rnc

ACKNOWLEDGEMENTS

Part of the work of Gerardo Espinosa–Pérez was developed during a sabbatical leave at LSS-SUPELEC supported by SUPELEC Foundation. Currently, his work is supported by DGAPA-UNAM (IN111211) and II-FI-UNAM (Grant 1111). The work of Dhruv Shah was supported by the Indo-French project No. 3602-1, under the aegis of IFCPAR. The authors want to thank Alain Glumineau and Robert Boisliveau (IRCCyN, France) for the computational code to generate the operator $\mathcal{A}$.

REFERENCES

1. Taylor D. Nonlinear control of electric machines: an overview. *IEEE Control Systems Magazine* 1994; **14**(6):41–51.
2. Dawson D, Hu J, Burg T. *Nonlinear Control of Electric Machinery*. Marcel Dekker: New York, USA, 1998.
3. Khorrami F, Krishnamurthy P, Melkote H. *Modeling and Adaptive Nonlinear Control of Electric Motors*. Springer: Heidelberg, 2003.
4. Nam K. *AC Motor Control and Electric Vehicle Applications*. CRC Press: UK, 2010.
5. Ortega R, Loria A, Nicklasson PJ, Sira-Ramírez H. *Passivity-based Control of Euler-Lagrange Systems*, Communications and Control Engineering. Springer-Verlag: Berlin, 1998.
6. Rajashekara K, Kawamura A, Matsuse K. *Sensorless Control of AC Motor Drives*. IEEE Press, 1996.
7. Ichikawa S, Tomita M, Doki S, Okuma S. Sensorless control of PMSM using on-line parameter identification based on system's identification theory. *IEEE Trans Industrial Electronics* 2006; **53**(2):363–373.
8. Ciabattoni L, Corradini ML, Grisostomi M, Ippoliti G, Longhi S, Orlando G. Adaptive extended Kalman filter for robust sensorless control of PMSM drives. *50th IEEE Conference on Decision and Control and European Control Conference*, Orlando, Florida, USA, December 12–15, 2011; 934–939.
9. Ortega R, Praly FL, Astolfi A, Lee J, Nam K. Estimation of rotor position and speed of permanent magnet synchronous motors with guaranteed stability. *IEEE Transaction on Control Systems Technology* 2011; **19**(2): 284–296.
10. Matsui N. Sensorless PM brushless DC motor drives. *IEEE Transactions on Industrial Electronics* 1996; **43**(2): 300–308.
11. Lee J, Hong J, Nam K, Ortega R, Astolfi A, Praly L. Sensorless control of surface-mount permanent magnet synchronous motors based on a nonlinear observer. *IEEE Transactions on Power Electronics* 2010; **25**(2): 290–297.
12. Astolfi A, Karagiannis D, Ortega R. *Nonlinear and Adaptive Control with Applications*, Communications and Control Engineering. Springer-Verlag: Berlin, 2007.
13. Ortega R, Garcia-Canseco E. Interconnection and damping assignment passivity-based control: a survey. *European Journal of Control* 2004; **10**:432–450.
14. Shah D, Ortega R, Astolfi A. Speed and load torque observer for rotating machines. *48th IEEE Conference on Decision and Control*, Shangai, P.R.China, December 16–18, 2009; 6143–6148.
15. Akrad A, Hilairet M, Ortega R, Diallo D. Interconnection and damping assignment approach for reliable pm synchronous motor control. *Colloquium On Reliability in Electromagnetic Systems*, Paris, France, 2007; 1–6.
16. Petrovic V, Ortega R, Stankovic A. Interconnection and damping assignment approach to control of PM synchronous motor. *IEEE Transactions on Control Systems Technology* 2001; **9**(6):811–820.
17. Fabio G, Miceli R, Rando C, Ricco–Galluzzo G. Back EMF sensorless-control algorithm for high-dynamic performance PMSM. *IEEE Transactions on Industrial Electronics* 2010; **57**(6):2092–2100.
18. Ezzat M, de Leon J, Gonzalez N, Glumineau A. Observer-controller scheme using high order sliding mode techniques for sensorless speed control of permanent magnet synchronous motor. *49th IEEE Conference on Decision and Control*, Atlanta, Georgia, USA, 2010; 4012–4017.
19. Tomei P, Verrelli CM. A nonlinear adaptive speed tracking control for sensorless permanent magnet step motors with unknown load torque. *International Journal of Adaptive Control and Signal Processing* 2008; **22**(3):266–288.
20. Ezzat M, Glumineau A, Plestan F. Sensorless speed control of a permanent magnet synchronous motor: high order sliding mode controller and sliding mode control observer. *8th IFAC Symposium on Nonlinear Control Systems*, Bologne, Italie, Septembre 01-03, 2010.
21. Nahid Mobarakeh B, Meibody–Tabar F, Sargos F. Robustness study of a model-based technique for mechanical sensorless control of PMSM. *PESC'01*, Vancouver, BC, Canada, June 2001; 811–816.
22. Marino R, Tomei P, Verrelli CM. Adaptive field-oriented control of synchronous motors with damping windings. *European Journal of Control* 2008; **14**(3):177–196.
23. Ibarra–Rojas S, Moreno J, Espinosa–Perez G. Global observability analysis of sensorless induction motors. *Automatica* 2004; **40**(6):1079–1085.
24. Basic D, Malrait F, Rouchon P. Euler–Lagrange models with complex currents of three-phase electrical machines and observability issues. *IEEE Transactions on Automatic Control* 2010; **55**(1):212–217.
25. Moreno JA, Espinosa–Pérez G. Sensorless PBC of induction motors: a separation principle from ISS properties. *46th IEEE Conference on Decision and Control*, New Orleans, Loussiana, USA, 2007; 6094–6099.
26. Ortega R, Espinosa G. Torque regulation of induction motors. *Automatica* 1993; **29**(3):621–633.

DOI: 10.1002/rnc

27. Chiasson J. *Modeling and High Performance Control of Electric Machines*. John Wiley & Sons: New Jersey, USA, 2005.
28. Krause PC. *Analysis of Electric Machinery*. McGraw Hill: New York, 1986.
29. Zaltni D, Naceur M, Ghanes M, Barbot JP. Observability analysis of PMSM. *2009 International Conference on Signals, Circuits and Systems*, Jerba, Tunisia, November 6–8, 2009; 1–6.
30. Organick EI. *A FORTRAN IV Primer*. Addison-Wesley: Massachusetts, USA, 1966.
31. van der Schaft AJ. $\mathcal{L}_2$*-Gain and Passivity Techniques in Nonlinear Control*. Springer-Verlag: Berlin, 2000.

DOI: 10.1002/rnc